Numerical Simulation of Concentration Gradient Generator Based on Cantor Fractal Principle

Huo, Xuyao

Faculty of Mechanical Engineering and Automation, Liaoning University of Technology, Jinzhou, Liaoning 121001, P.R. CHINA

Wang, Jinyuan

Department of Information Engineering, Chaoyang Teachers College, Chaoyang, Liaoning 12200, P.R. CHINA

Lv, Honglin

Faculty of Mechanical Engineering and Automation, Liaoning University of Technology, Jinzhou, Liaoning 121001, P.R. CHINA

Chen, Xueye*[+]

College of Transportation, Ludong University, Yantai, Shandong 264025, P.R. CHINA

ABSTRACT: *This paper mainly studies the design of a concentration gradient generator. Since the fractal principle has been shown to have unique geometric properties, we study the fractal principle together with the concentration gradient generator. We designed an obstacle based on the Cantor structure fractal applied the obstacle to the concentration gradient generator and then used the simulation software COMSOL Multiphysics 5.2a based on the finite element theory to carry out the numerical simulation. (a) The effect of fractal obstacle series on the concentration gradient, (b) the effect of microchannel height on the concentration gradient, and (c) the effect of different inlet velocities on the concentration gradient. A series of conclusions are obtained. The primary and secondary fractal obstacle has little influence on the concentration gradient. With the increase in the height of the microchannel, the change in the concentration gradient is small. The concentration gradient curve at different flow rates of the three-inlet concentration gradient generator shows a normal distribution trend. When the velocity decreases from 5×10^{-3} m/s to 1×10^{-5} m/s, the peak value of the curve decreases from 0.6 mol/L to about 0.35 mol/L. The concentration gradient curves at different flow rates of the two-inlet concentration gradient generator show a linear trend. When the velocity decreases from large 5×10^{-3} m/s to 1×10^{-5} m/s, the vertex value of the curve decreases from 1 to about 0.5 mol/L of complete mixing.*

KEYWORDS: *Concentration gradient generator; Structure design; Cantor Fractal; Numerical simulation.*

***** *To whom correspondence should be addressed.*

+ *E-mail: xueye_chen@126.com*

1021-9986/2023/5/1630-1638 *9/$/5.0*9

INTRODUCTION

Microfluidic chips have been widely used in biochemical and chemical engineering fields in recent years. Generating precise concentration gradients is greatly important in several research areas such as cell chemotaxis [1,2], cell cultures [3,4], dielectrophoresis phenomenon [5-7]. The concentration gradient generator can be prepared by three-dimensional printing or on the surface of Poly(dimethylsiloxane) (PDMS) [8]. Microfluidic systems can generate gradients in chemical composition and surface topography. This method is based on controlled diffusive mixing of species in solutions that are flowing laminarly, at low Reynolds number, inside a network of microchannels [9,10]. Microfluidic concentration gradient generator has a wide range of applications, such as the analysis of some conventional chemical reagents and cells [11]. Flow rate has a great influence on the concentration gradient and can precisely control the gradient profile [12]. The generation of gradients can have complex shapes in solution using microfluidic networks, and it is possible to generate spatially and temporally constant gradients extending over hundreds of micrometers and to maintain their shapes over long periods of time [13]. It is critical for a concentration gradient generator to effectively control of sample partially mixed. In recent years, we have made a series of studies on design [14], simulation [15,16], optimization [17], fabrication [18] of micromixers, micro direct methanol fuel cells [19] and micromixers actuated with magnetic nanomaterials [20].

Because fractal obstacles have obvious advantages on heat transfer and fluid transfer in rough microchannels [21]. *Chen et al.* [22] developed and analyzed numerically a model of laminar heat transfer in rough microchannels based on Cantor fractal characterization. The results indicate the laminar heat transfer in microchannels is also enhanced by roughness with a larger fractal dimension yielding more frequent variation in the surface profile even though at the same relative roughness. *Hong, Bo, et al.* [23] presented a concentration gradient generator based on a paper-based microfluidic device and cell culture microarrays for high-throughput drug screening. From the above study, we can find that the study of concentration gradient-generating micro-mixers is necessary. It plays an important role in areas such as drug screening. In the present study, we set up a baffle of Cantor fractal inside the microchannel of the concentration gradient generator. Although the theory of fractal geometry was born soon, research based on fractal principles can be applied to various fields. Its impact on several disciplines has been extremely significant. Many researchers have also started the research and application of fractal geometry, and its potential use and wide application prospects are impressive. It is believed that with the continuous research and exploration of experts from all parties, the applications brought by fractals will become more and more common in our daily lives.

In this article, our aim was to design a concentration gradient generator with Cantor fractal structure which can generate the concentration gradient with complex shapes by controlling flow velocity. This paper describes two gradient generators that can generate the approximate linear and secondary concentration gradient curves. Simultaneously, we analyze the effects of mesh number, fractal series, microchannel height, and inlet velocity on the concentration gradient curve.

DESIGN AND SIMULATION

Geometric structures

We first design an obstacle model. Fig.1 shows the design process of the obstacle. According to the Cantor fractal set structure, we design a simple fractal geometry model. This simple generation process as following:

(1) In the initial step, specify a straight line with a fixed length of L=1200μm.

(2) In the second step, the microchannel model begins at a height of 300μm. A straight line is divided into eight equal parts L_1=1/8L, L_1=150μm. The initial height of the barrier conforming to the Cantor fractal principle is 200μm. The primary fractal is shown in Fig.1(b).

(3) In the third step, the remaining lines are segmented in the same proportion L_2=1/8N, L_2=37.5μm, and the primary fractal obstacle will be divided into secondary fractal obstacles. The secondary fractal is shown in Fig.1(c).

Then we combine the obstacles with the microchannel. Two fractal obstacles are interlaced and set inside the microchannel. Then it is stretched by 3D software. Fig.2 shows the 3D structure of the Cantor concentration gradient generator.

Governing equations

The geometric structures of microchannels are imported in the COMSOL Multiphysics 5.2a software which is a numerical simulation software based

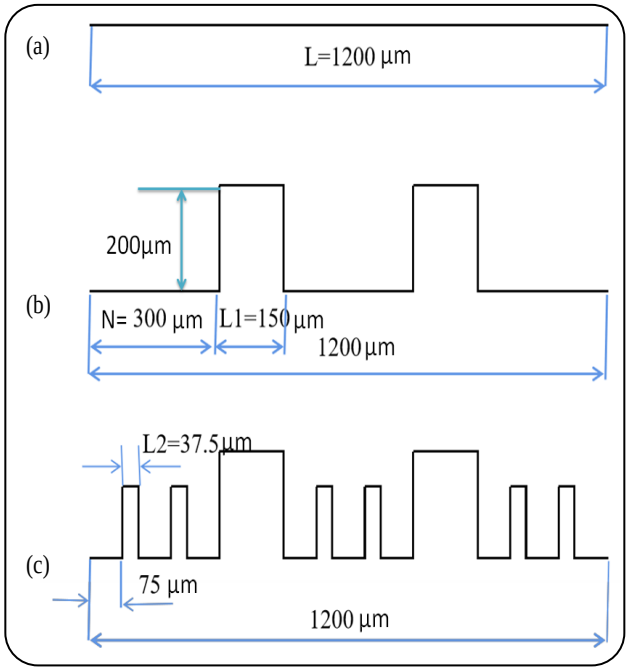

Fig. 1: Fractal structure design of imitating Cantor structure.

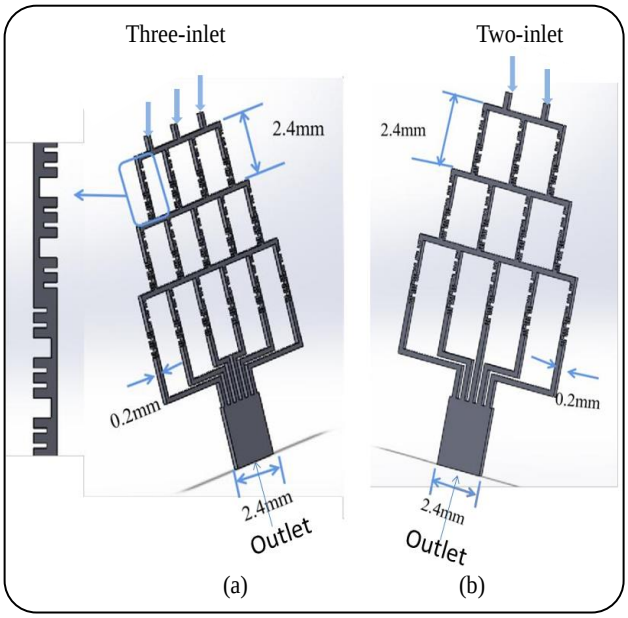

Fig.2: The basic structure of the concentration gradient generator with a different number of inlets. (a) three-inlet, (b) two-inlet.

on the finite element method. There are two governing equations as calculative tools in the simulation. The equations are shown as follows.

The governing equations for isothermal and incompressible Newtonian fluids in microchannels are continuity equation and Navier-Stokes equation, which can be expressed, respectively, in the following:

$$\nabla u = 0 \tag{1}$$

$$\rho \frac{\delta u}{\delta t} + \rho(u \cdot \nabla)u + \nabla p - \mu \nabla^2 u = 0 \tag{2}$$

Where u is the velocity vector, ρ the density, at the time, p the pressure and μ is the dynamic viscosity.

In order to investigate mixing effect in the microfluidic systems, the convection-diffusion equation can be used and described with Eq (3):

$$\frac{\delta c}{\delta t} + (u \cdot \nabla)c = D\nabla^2 \tag{3}$$

where c is the concentration, D is the diffusion coefficient and u is the flow velocity.

Because of short time for samples mixing, we only need to research the samples in steady state and time items in Eq (2) and Eq (3) which are negligible.

Finite element modeling

Finite element method is often used in the process of simulation experiment. In this paper, COMSOL Multiphysics 5.2a is used for numerical simulation analysis, and the results are accurate and reliable. The incompressible Navier-Stokes module and convection-diffusion module were chosen in the COMSOL Multiphysics software. The basic parameters are set as following. The microchannel sample was set to water because the viscosity and density of the medium were almost the same as that of water. The diffusion coefficient was fixed at 1×10^{-11} m^2/s to reduce the number of experimental variables. The concentration gradient generator with two-inlet enters the aqueous solution at the same flow rate, and the sample concentration of the generator with two-inlet are respectively set C_1=1mol/L and C_2=0mol/L. The sample concentration of the concentration with three-inlet are respectively set C_1=0mol/L and C_2=1mol/L, C_3=0mol/L respectively. A fluid dynamic boundary condition applied in the COMSOL Multiphysics is that there is no slip on all walls and the outlet is set at zero relative pressure.

Grid independence analysis

Fig. 3 shows the velocity curve at the outlet of the concentration gradient generator. The abscissa represents the height of the exit of the microchannel, and the ordinate represents the velocity on the section line at the exit. In the grid independence test, we use the same structure

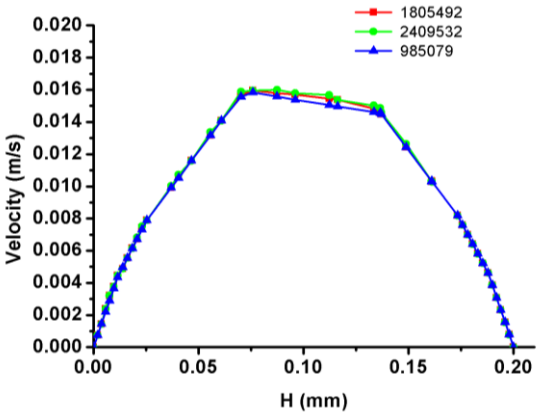

Fig. 3: Velocity curve at the outlet of the concentration gradient generator.

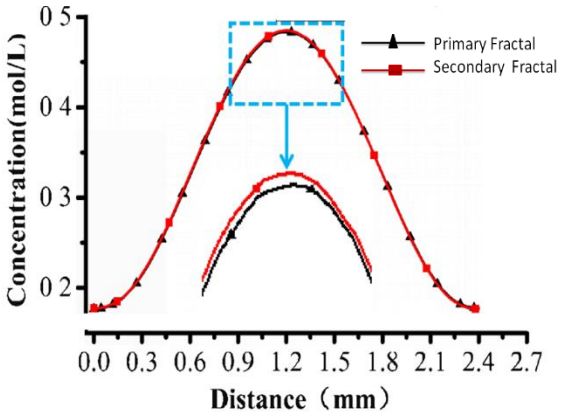

Fig.4: Concentration gradient curve of primary fractal obstacles and secondary fractal obstacles.

to analyze the grid independence. The number of grid cells indicated by the red curve in the figure is 1805492. The number of grid cells represented by the green curve is 2409532. The number of grid cells represented by the blue curve is 985079. As can be seen from Fig.3, the difference between the three curves is smaller with the increase in the number of meshes. The results show that the change of grid number has little effect on the concentration gradient generator. This is sufficient for the theoretical solution and analysis of the Cantor fractal concentration gradient generator based on the finite element method.

RESULTS AND DISCUSSION

Before the discussion, we found that applying the fractal principle to the design of the micromixer can improve the mixing performance of the micromixer and also have an impact on the fluid flow characteristics by reviewing the relevant literature [24]. Therefore, in this work, we design the concentration gradient generator based on the Cantor fractal principle.

The effect of fractal obstacle series on the concentration gradient

In this part, we compared the effect of the fractal obstacle series on the concentration gradient. The number of primary and secondary fractal obstacles in the design microchannels is two. There are Cantor fractal obstacles on both sides of the microchannel, they are arranged alternately, and the two adjacent fractals above and below are continuous. Fig.4 shows a comparison of the concentration gradient curves of the three-inlet concentration gradient generator with primary and secondary Cantor fractal barriers. Fig.5 shows the mixing effect of a three-inlet concentration gradient generator with primary and secondary Cantor fractal barriers. Combining the concentration curves and local enlargements of the concentration distributions in Figs. 5 and 6, it can be seen that the mixing effects of the primary fractionated micromixer and the secondary fractionated micromixer are extremely close to each other. This may be due to the unique structure of the concentration gradient type micromixer so that the concentration is minimally influenced by the shape of the baffle.

Fig.6 shows the comparison of the mixed concentration gradient curves of the two-inlet concentration gradient generator with a primary fractal obstacle and the two-inlet concentration gradient generator with a secondary fractal obstacle. Fig.7 shows the mixing effect of the two-inlet concentration gradient generator with a primary fractal obstacle and the two-inlet concentration gradient generator with a secondary fractal obstacle. It is obvious from Fig. 6 that the concentration variation curve of the dual inlet concentration gradient generator is approximately linearly decreasing. In contrast, the concentration change curve of the three-inlet concentration gradient generator has the shape of a quadratic convex function. This shows that the number of inlets can influence the fluctuation of the concentration curve.

Since the fractal principle has a unique geometric structure, the structure designed as a channel based on the Cantor fractal principle can have an effect on the flow characteristics of the fluid [25]. This further validates the need for this study.

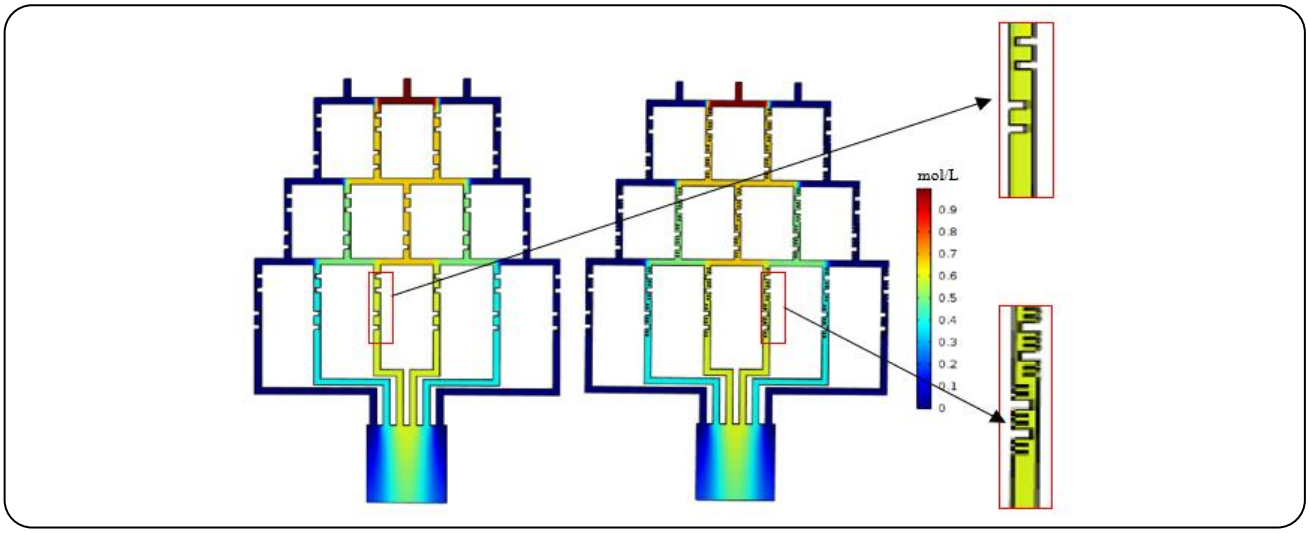

Fig. 5: Mixed effect diagrams of concentration gradient generator of primary and secondary fractal.

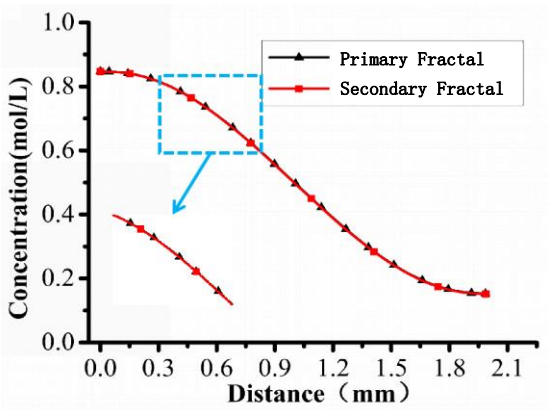

Fig.6: Concentration gradient curve of primary fractal obstacles and secondary fractal obstacles.

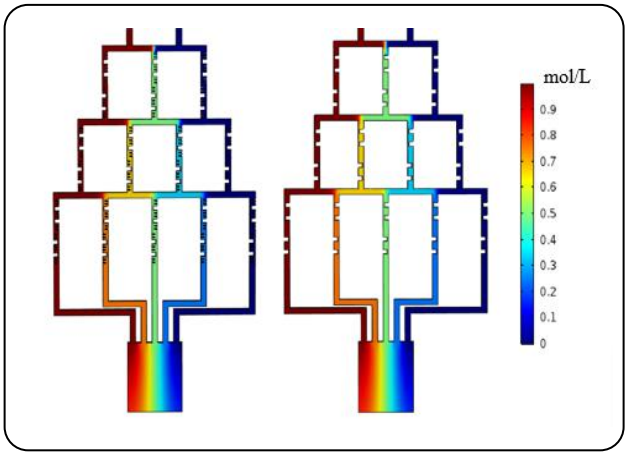

Fig. 7: Concentration gradient generator composed of primary fractal and secondary fractal.

From the above simulation results, it can be found that the solution in the mixing channel of the primary classification structure can be completely mixed under the same other conditions such as inlet velocity and inlet concentration. The mixing effect of the gradient generator with primary and secondary fractal obstacles is not much different. Considering that the more fractal number, the more complex the mesh division will be, the more computational cost of simulation will be, and the longer the calculation time will be. In order to save simulation time and computer resources, we choose a concentration gradient generator with a primary Cantor fractal structure for simulation analysis.

The effects of microchannel height on the concentration gradient

Since the inlet area of the microchannel affects the fluid flow energy [26], we guess that the height of the microchannel also affects the fluid flow energy. According to the above conclusion, the microchannel composed of primary fractal obstacles has the best mixing performance. Therefore, we will analyze and compare the effect of microchannels with different heights on the concentration gradient in this section. For this group, the inlet velocity is set to 0.0001 mm/s. The height of the microchannel is 100μm、200μm and 300μm, respectively. Fig.8 shows the concentration gradient curves of the three-inlet concentration gradient generator at different microchannel heights. Fig.9 shows the effect of concentration gradient of

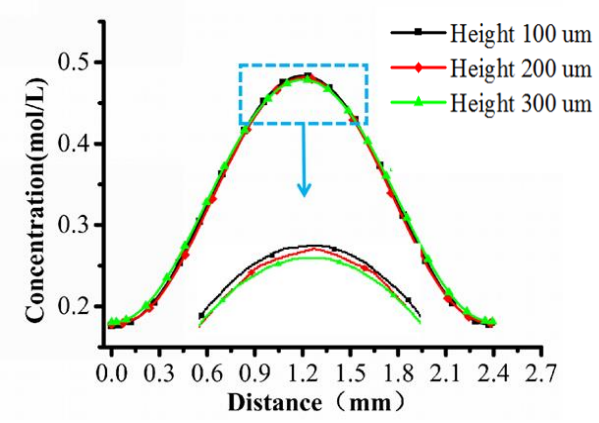

Fig. 8: Concentration gradient curve comparison of three different heights.

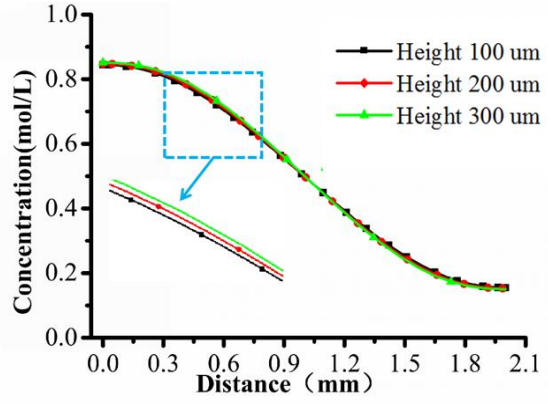

Fig. 10: Concentration gradient curve comparison of three different heights.

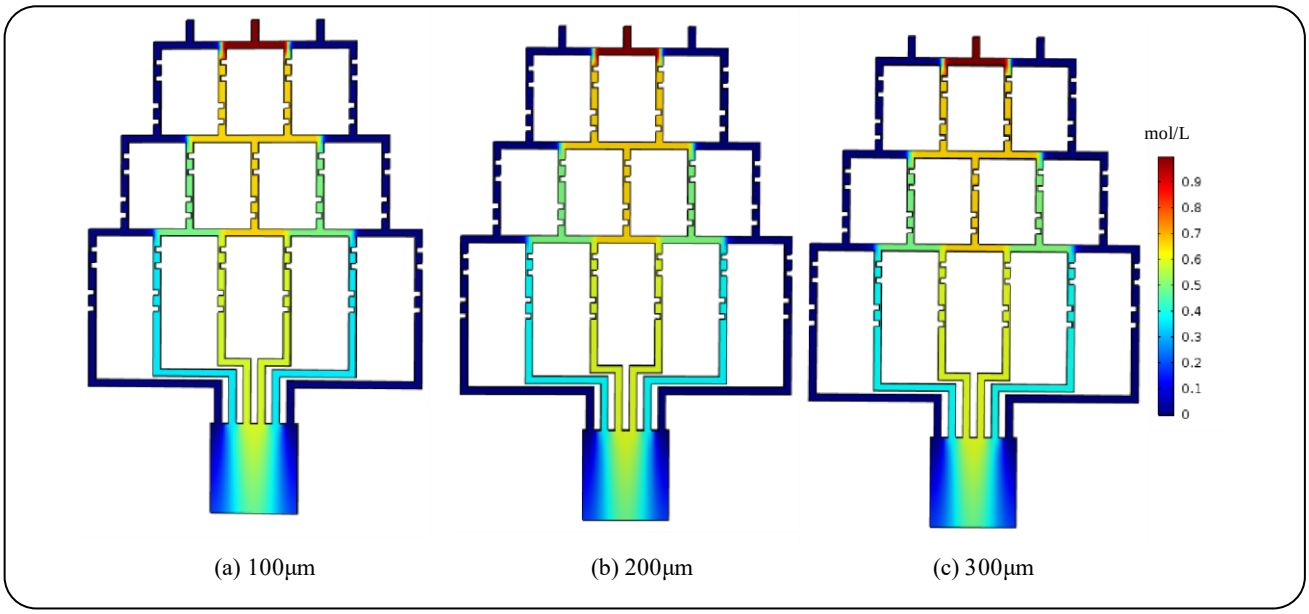

Fig.9: Mixing performance of three different heights.

the three-inlet concentration gradient generator at different microchannel heights.

Fig.10 shows the concentration gradient curves of the two-inlet concentration gradient generator at different microchannel heights. Fig.11 shows the effect of a concentration gradient of the two-inlet concentration gradient generator at different microchannel heights. As can be seen in Fig. 9, the concentration gradient generator with a height of 100μm is closest to 0.5 mol/L relative to the other two. This represents a better mixing capacity than the other two.

As can be seen from Fig.10 and Fig.11, under the same conditions, for the concentration gradient generator with two and three entrances. The increase in the height of the microchannel does not have too much effect on the concentration gradient, and the increase in the height of the microchannel will increase the number of meshes in the simulation. This increases the computational cost of the simulation, so the concentration gradient generator structure with a height of 100μm is finally selected.

The effect of different velocity on the concentration gradient

Different flow rates change the Reynolds number of the fluid, so the essence of the comparison velocity is to compare the effect of different Reynolds numbers on the

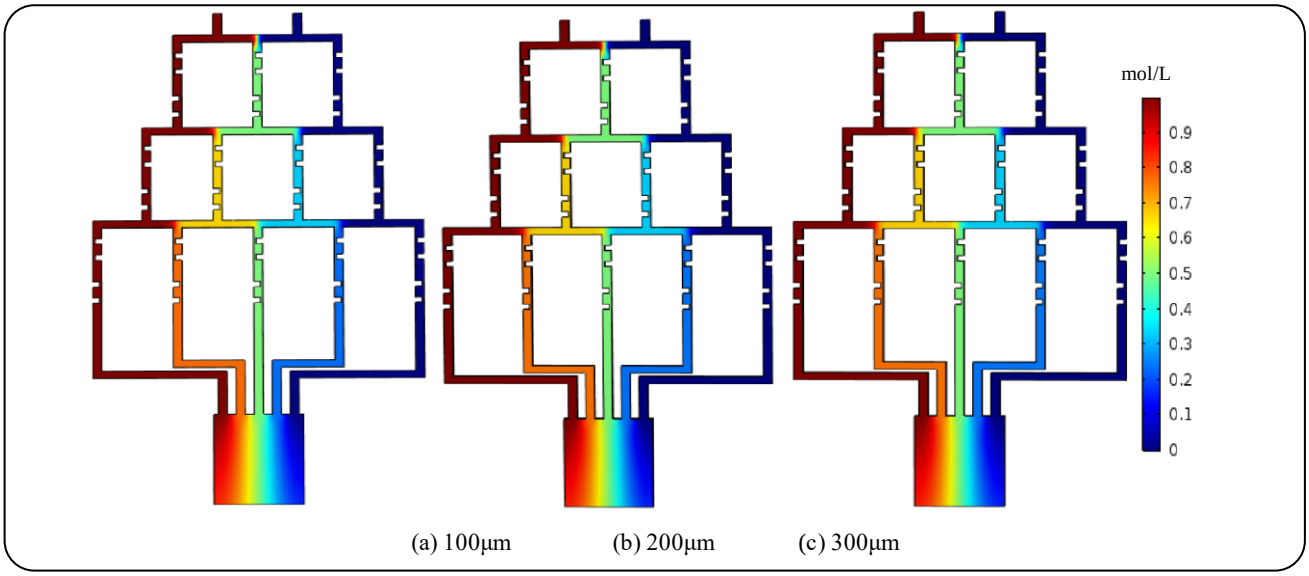

Fig.11: Mixing performance of three different height.

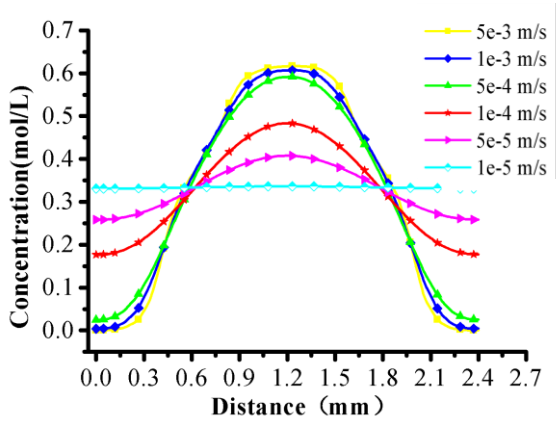

Fig. 12: Concentration gradient curve of the concentration gradient generator with three-inlet of at six different flow velocities.

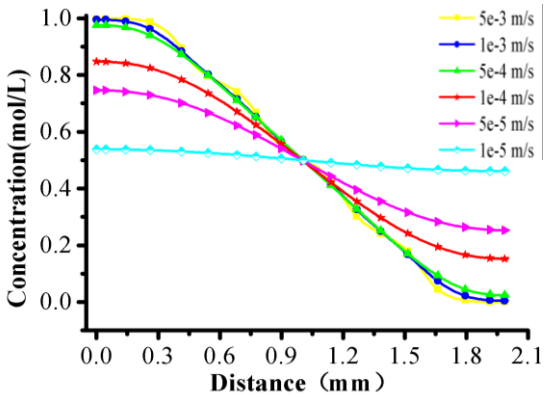

Fig. 13: Concentration gradient curve of the concentration gradient generator with two-inlet of at six different flow velocities.

concentration gradient. According to the analysis results of the above groups, an optimal microchannel structure can be obtained, which consists of two primary fractal obstacles with a height of 100μm, spacing 0μm and staggered distribution. In order to obtain more suitable velocity, more concentration gradient curves are achieved. On this basis, we continue to simulate and test the concentration gradient produced by the concentration gradient generator at six different flow rates from small to large. Fig.12 and Fig.13 show the concentration gradient curves of the two-inlet and three-inlet concentration gradient generators at six different, respectively.

Compared with the mixing efficiency of the concentration gradient generator at six different flow rates, it can be concluded from Fig.12 and Fig.13 that the concentration gradient curve at different flow rates of the three-inlet concentration gradient generator shows a normal distribution trend. When the velocity decreases from 5×10^{-3} m/s to 1×10^{-5} m/s, the peak value of the curve decreases from 0.6 mol/L to about 0.35 mol/L. The concentration gradient curve of the double-inlet concentration gradient generator at different flow rates is close to a linear trend. When the velocity decreases from large 5×10^{-3} m/s to 1×10^{-5} m/s, the vertex value of the curve decreases from 1 to about 0.5 mol/L of complete

mixing. When the velocity is 1×10^{-5} m/s, the curve has almost no gradient. It indicates that the solution reaches complete mixing in the outlet region.

CONCLUSIONS

The concentration gradient generator based on Cantor fractal structure is mainly introduced in this paper, and the effects of mesh number, fractal series, microchannel height and inlet velocity on the concentration gradient curve are studied. Since the Cantor fractal structure can obviously increase the mixing efficiency of the fluid, the applied fractal structure Cantor in the mixed channel region of the concentration gradient generator. The simulation results show that firstly, the increase of the number of grids does not have too much effect on the concentration gradient under the number of three grids tested. So, the number of grids with the least number of grids is finally selected, that is, the number of grids of two-inlet and three-inlet concentration gradient generators is 1.58×10^{5} and 1.3×10^{5} respectively, which can reduce the simulation time. Secondly, the increase of fractal series and microchannel height also does not have too much effect on the concentration gradient, and the increase of fractal series and microchannel height will increase the number of meshes in the simulation, thus increasing the computational cost of the simulation. So the concentration gradient generator structure with a fractal series and a height of 100μm is finally selected. Finally, through the simulation study of changing the inlet flow rate, we can find that the concentration gradient curve under different flow rates of the three-inlet concentration gradient generator is normally distributed. When the velocity is from large to small, from 5×10^{-3} m/s to 1×10^{-5}, the peak value of the curve decreases continuously, from 0.6mol/L to about 0.35mol/L. The concentration gradient curves at different flow rates of the two-inlet concentration gradient generator show a linear trend. When the velocity is from large to small, from 5×10^{-3} m/s to 1×10^{-5}m/s, the vertex value of the curve decreases continuously, from 1 mol/L to about 0.5 mol/L of complete mixing. When the velocity is 1×10^{-5} m/s, the curve has almost no gradient, indicating that the solution reaches complete mixing in the outlet region. With the development of science and technology, the application of concentration gradient generator is more and more widely. At present, the concentration gradient generator can be used in the fields of cell screening, chemical reagent detection, and the interaction of dielectric electrophoresis.

Acknowledgments

This work was supported by the Young Taishan Scholars Program of Shandong Province of China (tsqn202103091), Special Supporting Funds for Leading Talents at or Above the Provincial Level in Yantai City.

Received ; May. 23, 2023 ; Accepted : Sep. 18, 2022

REFERENCES

[1] Zhan X., Chen G., Jing D., Optimal Analysis of the Hydraulic and Mixing Performances of Symmetric T-Shaped Rectangular Microchannel Mixer, *Fractals*, **29(2)**: 2150042 (2021).

[2] Liu F., Jing D., Combined Electroosmotic and Pressure Driven Flow in Tree-Like Microchannel Network, *Fractals*, **29(5)**: 2150110(2021).

[3] Li Y., Xuan J., Hu R., Zhang P., Lou X., Yang Y., Microfluidic Triple-Gradient Generator For Efficient Screening of Chemical Space, *Talanta*, **204**: 569-575 (2019).

[4] Zhao X., Yan X., Li Y., Liu B.F., Static Pressure-Driven Microfluidic Gradient Generator for Long-Term Cell Culture and Adaptive Cytoprotection Analysis, *Microfluidics and Nanofluidics*, **23(5)**: 1-10(2019).

[5] Rahimi M., Aghel B., Hatamifar B., Akbari M., Alsairafi A., CFD Modeling of Mixing Intensification Assisted with Ultrasound Wave in a T-Type Microreactor, *Chemical Engineering and Processing: Process Intensification*, **86**: 36-46 (2014).

[6] Zhou T., Ji X., Shi L., Hu N., Li T., Dielectrophoretic Interactions of Two Rod-Shaped Deformable Particles under DC Electric Field, *Colloids and Surfaces A: Physicochemical and Engineering Aspects*, **607**: 125493(2020).

[7] Zhou T., Ji X., Shi L., Zhang X., Deng Y., Joo S.W., Dielectrophoretic Choking Phenomenon in a Converging-Diverging Microchannel for Janus Particles, *Electrophoresis*, **40(6)**: 993-999 (2019).

[8] Zhou B., Gao Y., Tian J., Tong R., Wu J., Wen W., Preparation of Orthogonal Physicochemical Gradients on PDMS Surface Using Microfluidic Concentration Gradient Generator, *Applied Surface Science*, **471**: 213-221 (2019).

[9] Kumaran V., Bandaru P., Ultra-Fast Microfluidic Mixing by Soft-Wall Turbulence, *Chemical Engineering Science*, **149**: 156-168 (2016).

[10] Shenoy D.V., Shadloo M.S., Peixinho J., Hadjadj A., Direct Numerical Simulations of Laminar and Transitional Flows in Diverging Pipes, *International Journal of Numerical Methods for Heat & Fluid Flow*, (2019).

[11] Liu X., Jia Y., Han Z., Hou Q., Zhang W., Zheng W., Jiang X., Integrating a Concentration Gradient Generator and a Single-Cell Trapper Array for High-Throughput Screening the Bioeffects of Nanomaterials, *Angewandte Chemie International Edition*, **60(22)**: 12319-12322 (2021).

[12] Gidde R.R., Pawar P.M., Ronge B.P., Misal N.D., Kapurkar R.B., Parkhe A.K., Evaluation of the Mixing Performance in a Planar Passive Micromixer with Circular and Square Mixing Chambers, *Microsystem Technologies*, **24(6)**: 2599-2610 (2018).

[13] Chen X., Zhao Z., Numerical Investigation on Layout Optimization of Obstacles in a Three-Dimensional Passive Micromixer, *Analytica Chimica Acta*, **964**: 142-149 (2017).

[14] Shi X., Huang S., Wang L., Li F., Numerical Analysis Of Passive Micromixer With Novel Obstacle Design, *Journal of Dispersion Science and Technology*, **42(3)**: 440-456 (2021).

[15] Tofteberg T., Skolimowski M., Andreassen E., Geschke O., A Novel Passive Micromixer: Lamination in a Planar Channel System, *Microfluidics and Nanofluidics*, **8(2)**: 209-215 (2010).

[16] Zhao S., Chen C., Zhu P., Xia H., Shi J., Yan F., Shen R., Passive Micromixer Platform for Size-and Shape-Controllable Preparation of Ultrafine HNS, *Industrial & Engineering Chemistry Research*, **58(36)**: 16709-16718 (2019).

[17] Bayareh M., Ashani M.N., Usefian A., Active and Passive Micromixers: A Comprehensive Review, *Chemical Engineering and Processing-Process Intensification*, **147**: 107771 (2020).

[18] Jothimuthu P., Bhagat A.A.S., Papautsky I., PhotoPDMS: Photodefinable PDMS for Rapid Prototyping. In 2008 17th Biennial University/Government/Industry Micro/Nano Symposium (pp. 183-186). IEEE. (2008).

[19] Raza W., Hossain S., Kim K.Y., A Review of Passive Micromixers with a Comparative Analysis, *Micromachines*, **11(5)**: 455 (2020).

[20] Ruijin W., Beiqi L., Dongdong S., Zefei Z., Investigation on the Splitting-Merging Passive Micromixer Based on Baker's Transformation, *Sensors and Actuators B: Chemical*, **249**: 395-404 (2017).

[21] Jing D., Yi Sh., Electroosmotic Flow in Tree-Like Branching Microchannel Network, *Fractals*, **27(6)**: 1950095 (2019).

[22] Chen X., Shen J., Numerical Analysis of Mixing Behaviors of Two Types of E-Shape Micromixers, *International Journal of Heat and Mass Transfer*, **106**: 593-600 (2017).

[23] Hong B., Xue P., Wu Y., Bao J., Chuah Y.J., Kang Y., A Concentration Gradient Generator on a Paper-Based Microfluidic Chip Coupled with Cell Culture Microarray for High-Throughput Drug Screening. *Biomedical Microdevices*, **18(1)**: 1-8 (2016).

[24] Shah I, Aziz S, Soomro A M, et al. Numerical and Experimental Investigation of Y-Shaped Micromixers with Mixing Units Based on Cantor Fractal Structure for Biodiesel Applications, *Microsystem Technologies*, **27(5)**: 2203-2216 (2021).

[25] Kim K., Shah I., Ali M., Aziz Sh., Khalid M.A., Kim Y.S., Choi K.H., Experimental and Numerical Analysis of Three Y-Shaped Split and Recombination Micromixers Based on Cantor Fractal Structures, *Microsystem Technologies*, **26(6)**: 1783-1796 (2020).

[26] Shakaib M., Fatima U., A Numerical Study for the Effects of Narrow Channel Dimensions on Pressure Drop and Mass Transfer Performance of a Mixer Device, *Iranian Journal of Chemistry and Chemical Engineering (IJCCE)*, **41(5)**: 1727-1739 (2022).